Nonlocal damping of spin waves in a magnetic insulator induced by normal, heavy, or altermagnetic metallic overlayer: A Schwinger-Keldysh field theory approach

Felipe Reyes-Osorio and Branislav K. Nikolić[*]

Department of Physics and Astronomy, University of Delaware, Newark, Delaware 19716, USA

Understanding spin wave (SW) damping and how to control it to the point of being able to amplify SW-mediated signals is one of the key requirements to bring envisaged magnonic technologies to fruition. Even widely used magnetic insulators with low magnetization damping in their bulk, such as yttrium iron garnet, exhibit a *100-fold increase* in SW damping due to inevitable contact with metallic layers in magnonic circuits, as observed in very recent experiments [Bertelli *et al.*, Adv. Quantum Technol. **4**, 2100094 (2021)] mapping SW damping in a spatially resolved fashion. Here, we provide a microscopic and rigorous understanding of *wave-vector-dependent* SW damping using the extended Landau-Lifshitz-Gilbert equation with a *nonlocal damping tensor* instead of conventional local scalar Gilbert damping, as derived from Schwinger-Keldysh nonequilibrium quantum field theory. In this picture, the origin of nonlocal magnetization damping and thereby induced wave-vector-dependent SW damping is the interaction of localized magnetic moments of a magnetic insulator with conduction electrons from the three different types of metallic overlayers examined: normal, heavy, and altermagnetic. Due to the spin-split energy-momentum dispersion of conduction electrons in the latter two cases, the nonlocal damping is anisotropic in spin and space, and it can be dramatically reduced by changing the relative orientation of the two layers when compared to the usage of normal metal overlayer.

I. INTRODUCTION

Spin wave (SW) or magnon damping is a problem of great interest for both basic and applied research. For basic research, its measurements [1–4] can reveal microscopic details of boson-boson or boson-fermion quasiparticle interactions in solids, such as magnon-magnon interactions (as described by second-quantized Hamiltonians containing products of three or more bosonic operators [5,6]), which are frequently encountered in antiferromagnets [4,5] and quantum spin liquids [7,8], wherein they play a much more important role [9] than boson-boson interactions in other condensed phases, like anharmonic crystalline lattices or superfluids [5]; magnon-phonon interactions [3], which are especially relevant for recently discovered two-dimensional magnetic materials [2]; and magnon-electron interactions in magnetic metals [1,10–14]. For the envisaged magnon-based digital and analog computing technologies [15–19], understanding magnon damping makes it possible to develop schemes to suppress [20] it and, furthermore, achieve amplification of nonequilibrium fluxes of magnons [21–24]. In fact, overcoming damping and achieving amplification is the *key* to enabling complex magnon circuits in which, e.g., a logic gate output must be able to drive the input of multiple follow-up gates.

Let us recall that the concept of a SW was introduced by Bloch [25] as a wavelike disturbance in the local magnetic ordering of a magnetic material. The quanta [6] of energy of SWs of frequency ω behave as quasi-particles called magnons, each of which carries energy $\hbar\omega$ and spin $\hbar$. In regard to terminology, we note that in magnonics [15] a SW is often used for excitations driven by antennas [26–29] and/or described by the classical Landau-Lifshitz-Gilbert (LLG) equation [10,11,30,31], whereas a magnon is used for the quantized version of the same excitation [5], or these two terms are used interchangeably.

In particular, experiments focused on SW damping in metallic ferromagnets have observed [1] its dependence on the wave vector $\mathbf{q}$, which cannot be explained by using the standard LLG equation [30,31], $\partial_t \mathbf{M}_n = -\mathbf{M}_n \times \mathbf{B}_n^{\text{eff}} + \alpha_G \mathbf{M}_n \times \partial_t \mathbf{M}_n$ (where $\partial_t \equiv \partial/\partial t$), describing the dynamics of localized magnetic moments (LMMs) $\mathbf{M}_n$ at site n of a crystalline lattice (also used in atomistic spin dynamics [30]) viewed as classical vectors of unit length. This is because α_G, as the Gilbert damping parameter [32,33], is a *local scalar* (i.e., position-independent constant). Instead, various forms of spatially *nonuniform* (i.e., coordinate-dependent) and *nonlocal* (i.e., magnetization-texture-dependent) damping due to conduction electrons have been proposed [10,11,34–36] or extracted from first-principles calculations [37] to account for observed wave-vector-dependent damping of SWs, such as $\propto q^2$ ($q = |\mathbf{q}|$) measured in Ref. [1]. The nonlocal damping terms require neither spin-orbit coupling (SOC) nor magnetic disorder scattering, in contrast to α_G, which is considered to vanish [38] in their absence.

Thus, in magnonics, it has been considered [39] that the usage of magnetic insulators, such as yttrium iron garnet (YIG) exhibiting ultralow $\alpha_G \simeq 10^{-4}$ (achieved on a proper substrate [40]), is critical to evade much larger and/or

_____

[*]Contact author: bnikolic@udel.edu

nonlocal damping of SWs found in ferromagnetic metals. However, very recent experiments [26–29] have observed a *100-fold* increase of SW damping in the segment of a YIG thin film that was covered by a metallic overlayer. Such spatially resolved measurement [26] of SW damping was made possible by the advent of quantum sensing based on nitrogen vacancy (NV) centers in diamond [41], and it was also subsequently confirmed by other methods [27–29]. Since excitation, control, and detection of SWs require coupling YIG to metallic electrodes [15], understanding the origin of and means to control and suppress a large increase in SW damping underneath a metallic overlayer is crucial for realizing magnonic technologies.

To explain their experiments, the authors of Refs. [26–29] employed the LLG equation with *ad hoc* introduced terms (such as effective magnetic field due to SW-induced eddy currents within a metallic overlayer [26]) that fit their experimental data (see Appendix B). This approach is nonuniversal and unsatisfactory as it usually can only partially explain experimental data [42]. For example, simple renormalization of α_G, as attempted in Ref. [26], *cannot* [36] properly capture the wave-vector-dependence [1,11,26] of SW damping, while postulating forms of spatially dependent nonlocal damping [10,11,34–36] leads to many ambiguous choices [35]. A more microscopic route was taken in Refs. [43,44] using the picture of spin angular momentum loss via spin pumping, but the authors predicted only a modest $\lesssim$2-fold increase of SW damping (see Appendix A) that is independent of the wave vector at small q, thereby *contradicting the 100-fold* increase found experimentally [26] and sensitive dependence on small wave vector values.

In contrast, in this paper we employ the recently derived *extended* LLG equation,

$$\partial_t \mathbf{M}_n = -\mathbf{M}_n \times \mathbf{B}_n^{\text{eff}} + \mathbf{M}_n \times \sum_{n'} (\alpha_G \delta_{nn'} + \lambda_{\mathbf{R}}) \cdot \partial_t \mathbf{M}_{n'},$$
(1)

with all terms obtained [45] microscopically from Schwinger-Keldysh nonequilibrium quantum field theory [46] and confirmed [45] via exact quantum-classical numerics [47–50]. It includes nonlocal damping as the third term on the right-hand side (RHS), where its nonlocality is signified by the dependence on $\mathbf{R} = \mathbf{r}_n - \mathbf{r}_{n'}$, where $\mathbf{r}_n$ is the position vector of lattice site n. The Schwinger-Keldysh field theory (SKFT), commonly used in high-energy physics and cosmology [51–53], allows one to integrate out unobserved degrees of freedom, such as the conduction electrons in the setup in Fig. 1, leaving behind a time-retarded dissipation kernel [48,54,55] that encompasses electronic effects on the remaining degrees of freedom. This approach then rigorously yields an effective equation for *only LMMs*, such as Eq. (1) [45,55], which bypasses the need for adding [1,26,42] phenomenological wave-vector-dependent terms to the standard LLG equation. In our approach, the nonlocal damping is extracted from the time-retarded dissipation kernel [45].

The paper is organized as follows. Equation (1) is applied to a setup depicted in Fig. 1 in which conduction electron spins from three different choices of metallic overlayers are assumed to interact with LMMs of a ferromagnetic insulator (FI) at the interface via *sd* exchange interaction of strength
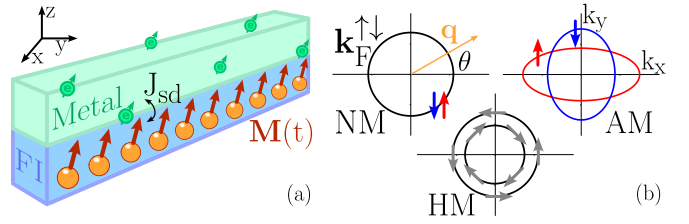

FIG. 1. (a) Schematic view of bilayers where a metallic overlayer covers the top surface of a magnetic insulator, as often encountered in spintronics and magnonics [15,39]. Three different energy-momentum dispersions of conduction electrons at the interface are considered, with their Fermi surfaces shown in (b): a normal metal (NM), a heavy metal (HM) with Rashba SOC [56,57], and an altermagnetic metal (AM) [58,59], with the latter two being spin split. The relative alignment of the layers is labeled by an angle θ [58,59], meaning that the wave vector $\mathbf{q}$ of SWs within the FI is at an angle θ away from the k_x axis.

J_{sd}, as well as possibly underneath the top surface of the FI because of an electronic evanescent wave function penetrating into it. Note that the FI/normal metal (NM) bilayer directly models recent experiments [26] in which the FI was a thin film of YIG, the NM was Au and SW damping within the FI was quantified using quantum magnetometry via NV centers in diamond. Next, a FI/heavy metal (HM) bilayer, such as YIG/Pt [20,29], is frequently encountered in various spintronics and magnonics phenomena [15,39]. Finally, due to the recent explosion of interest in altermagnets [58,59], FI/altermagnetic metal (AM) bilayers, such as YIG/RuO$_2$, have been explored experimentally[1] to characterize RuO$_2$ as a spin-to-charge conversion medium [63].

II. SKFT-BASED THEORY OF SW DAMPING IN FI/METAL BILAYERS

The nonlocal damping [45] $\lambda_{\mathbf{R}}$ in the third term on the RHS of the extended LLG equation (1) stems from the backaction of conduction electrons responding nonadiabatically [48,64]—i.e., with the electronic spin expectation value $\langle \hat{\mathbf{s}}_n \rangle$ always lagging behind the LMM which generates spin torque [65] $\propto \langle \hat{\mathbf{s}}_n \rangle \times \mathbf{M}_n$—to the dynamics of LMMs. It is, in general, a nearly symmetric 3×3 tensor whose components are given by [45]

$$\lambda_{\mathbf{R}}^{\alpha\beta} = -\frac{J_{sd}^2}{2\pi} \int d\varepsilon \frac{\partial f}{\partial \varepsilon} \text{Tr}[\sigma^\alpha A_{nn'} \sigma^\beta A_{n'n}].$$
(2)

Here, $f(\varepsilon)$ is the Fermi function, $\alpha, \beta = x, y, z, \sigma^\alpha$ is the Pauli matrix, and $A(\varepsilon) = i[G^R(\varepsilon) - G^A(\varepsilon)]$ is the spectral function in the position representation obtained from the retarded and advanced Green's functions (GFs) $G^{R/A}(\varepsilon) = (\varepsilon - H \pm i\eta)^{-1}$. Thus, the calculation of $\lambda_{\mathbf{R}}$ requires only an electronic

---

[1]Note that recent experimental [60] and theoretical [61] scrutiny finds RuO$_2$ to be nonmagnetic in bulk form, but remains an AM metal in the few-atomic-layer form [62]. Thus, these developments do not affect our study focused on a bilayer structure, as well as results for wave-vector-dependent SW damping due to generic energy-momentum dispersion of an AM metal.

Hamiltonian H as input, which makes the theory fully microscopic (i.e., Hamiltonian based). In order to arrive at closed expressions for the nonlocal damping tensor, we employ simple model Hamiltonians; nevertheless, realistic materials can be treated by using the Hamiltonian input from first-principles calculations (as explained in Ref. [45]). Although the SKFT-based derivation [45] yields an additional antisymmetric term not displayed in Eq. (2), this term vanishes if the system has inversion symmetry. Even when this symmetry is broken, like in the presence of SOC, the antisymmetric component is often orders of magnitude smaller [55]; therefore, we neglect it. The first term on the RHS of the extended LLG equation (1) is the usual one [30,31], describing precession of LMMs in the effective magnetic field $\mathbf{B}_n^{\text{eff}}$, which is the sum of both internal and external ($B_{\text{ext}}\mathbf{e}_z$) fields. It is obtained as $\mathbf{B}_n^{\text{eff}} = -\partial\mathcal{H}/\partial\mathbf{M}_n$ where $\mathcal{H}$ is the classical Hamiltonian of LMMs:

$$\mathcal{H} = -J\sum_{\langle nn'\rangle}\mathbf{M}_n\cdot\mathbf{M}_{n'} + \frac{K}{2}\sum_n\left(M_n^z\right)^2 - B_{\text{ext}}\sum_n M_n^z. \quad (3)$$

Here, we use $g = 1$ for the gyromagnetic ratio, which simplifies Eq. (1); J is the Heisenberg exchange coupling between the nearest-neighbor sites, and K is the magnetic anisotropy.

When the nonlocal damping tensor $\lambda_\mathbf{R}$ is proportional to the 3×3 identity matrix $\mathcal{I}_3$, a closed formula for the SW dispersion can be obtained via hydrodynamic or linear spin wave theory [66]. In this theory, the localized spins in Eq. (1), $\mathbf{M}_n = (\text{Re}\,\phi_n, \text{Im}\,\phi_n, 1 - m)^T$, are expressed using complex field ϕ_n and uniform spin density $m \ll 1$. Then, using the SW ansatz $\phi_n(t) = \sum_\mathbf{q} U_\mathbf{q} e^{i(\mathbf{q}\cdot\mathbf{r}_n - \omega_\mathbf{q}t)}$, we obtain the dispersion relation for the SWs,

$$\omega_\mathbf{q} = (Jq^2 + K - B)[1 + i(\alpha_G + \tilde{\lambda}_\mathbf{q})], \quad (4)$$

where $\mathbf{q}$ is the wave vector and ω is the frequency. The damping of the SW in the linear regime is then given by the imaginary part of the dispersion in Eq. (4), $\Gamma_\mathbf{q}^{\text{linear}} \equiv \text{Im}\,\omega_\mathbf{q}$. It is composed of contributions from the local scalar Gilbert damping α_G and the Fourier transform of the nonlocal damping tensor, $\tilde{\lambda}_\mathbf{q} = \int d\mathbf{r}_n \lambda_{\mathbf{r}_n} e^{i\mathbf{q}\cdot\mathbf{r}_n}$.

III. RESULTS FOR A FI/NM BILAYER

We warm up by extracting $\Gamma_\mathbf{q}$ for the simplest of the three cases in Fig. 1, a one-dimensional (1D) FI chain under a 1D NM overlayer with spin-degenerate quadratic electronic energy-momentum dispersion, $\epsilon_{\mathbf{k}\sigma} = t_0 k_x^2$, where $t_0 = \hbar^2/2m$. The GFs and spectral functions in Eq. (2) can be calculated in the momentum representation, yielding $\lambda_R^{\text{1D}} = \frac{2J_{sd}^2}{\pi v_F^2}\cos^2(k_F R)\mathcal{I}_3$, where v_F is the Fermi velocity, $R \equiv |\mathbf{R}|$, and k_F is the Fermi wave vector. Moreover, its Fourier transform, $\tilde{\lambda}_q = \frac{2J_{sd}^2}{v_F^2}[\delta(q) + \delta(q - 2k_F)/2]$, dictates additional damping to SWs of wave vector $q = 0, \pm 2k_F$. Although the Dirac delta function in this expression is unbounded, this unphysical feature is an artifact of the low-amplitude, $m \ll 1$, approximation within the hydrodynamic approach [66]. The features of such wave-vector-dependent damping in one dimension can be *corroborated* via TDNEGF+LLG (TDNEGF stands for time-dependent nonequilibrium GF [67]) numerically exact simulations [47–50] of a finite-size nanowire, similar to the setup depicted in Fig. 1(a) but sandwiched between two NM
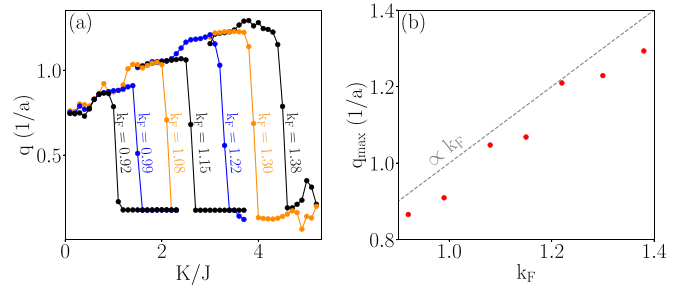

FIG. 2. (a) Wave vector q of a SW generated by injecting spin-polarized current in TDNEGF+LLG simulations of the NM overlayer on the top of the 1D FI [Fig. 1(a)] as a function of anisotropy K [Eq. (3)] for different electronic Fermi wave vectors k_F. (b) Maximum wave vector q_{max} of SWs that can be generated by current injection [23,68] before wave-vector-dependent SW damping becomes operative, as signified by the drop around k_F in curves plotted in (a).

semi-infinite leads. For example, by exciting SWs via injection of a spin-polarized current into the metallic overlayer of such a system, as pursued experimentally in spintronics and magnonics [23,68], we find in Fig. 2(a) that the wave vector q of a thereby excited coherent SW increases with increasing anisotropy K. However, the maximum wave vector q_{max} is limited by k_F [Fig. 2(b)]. This means that SWs with $q \gtrsim k_F$ are subjected to additional damping, inhibiting their generation. Although our analytical results predict extra damping at $q = 2k_F$, finite-size effects and the inclusion of semi-infinite leads in TDNEGF+LLG simulations lower this cutoff to k_F.

Since SW experiments are conducted on higher-dimensional systems, we also investigate damping of SWs in a two-dimensional (2D) FI/NM bilayer. The electronic energy-momentum dispersion is then $\epsilon_{\mathbf{k}\sigma} = t_0(k_x^2 + k_y^2)$, and the nonlocal damping and its Fourier transform are given by

$$\lambda_R^{\text{NM}} = \frac{k_F^2 J_{sd}^2}{2\pi v_F^2}J_0^2(k_F R)\mathcal{I}_3, \quad (5)$$

$$\tilde{\lambda}_q^{\text{NM}} = \frac{k_F J_{sd}^2 \Theta(2k_F - q)}{2\pi v_F^2 q\sqrt{1 - (q/2k_F)^2}}, \quad (6)$$

where $J_n(x)$ is the nth Bessel function of the first kind and $\Theta(x)$ is the Heaviside step function. The nonlocal damping in Eqs. (5) and (6) is plotted in Fig. 3(a), showing a realistic decay with increasing R, in contrast to the unphysical infinite range found in the 1D case. Additionally, SW damping in Eq. (6) is operative for wave vectors $0 \leqslant q \leqslant 2k_F$, again diverging for $q = 0, 2k_F$ due to artifacts of hydrodynamic theory [66]. Therefore, the unphysical divergence can be removed by going back to the discrete lattice and numerically solving a system of coupled LLG equations (1) where $\lambda_\mathbf{R}$ in two dimensions is used [45]. From the exponential decay of the initial SW amplitude in such numerical solutions, we extract the wave-vector-dependent SW damping $\Gamma_\mathbf{q}$, plotted as solid curves in Fig. 3(e). Note that SW damping obtained in this fashion includes nonlinear effects such as magnon-magnon interaction. In this numerical treatment we use $n = 1$–100 LMMs; $k_F = 0.5a^{-1}$, where a is the lattice spacing; $k_F^2 J_{sd}^2/2\pi v_F^2 = \eta = 0.1$; $K = 0$; $B_{\text{ext}} = 0.1J$; and $\alpha_G = 0.1$.
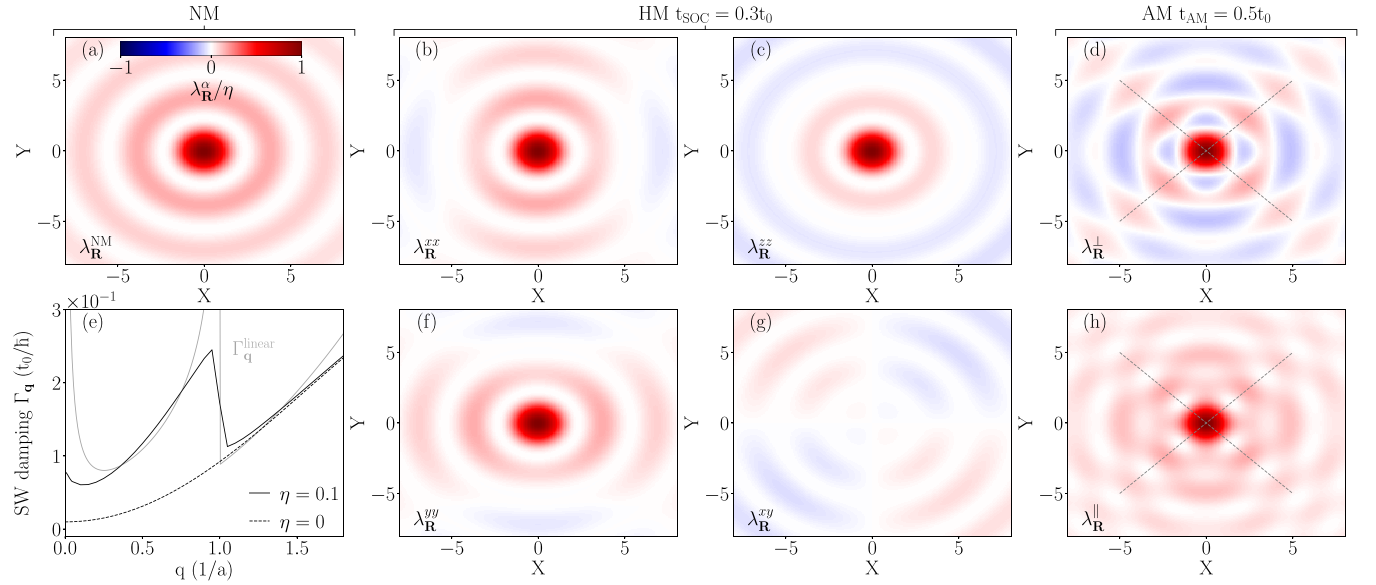
FIG. 3. (a)–(d) and (f)–(h) Elements of the SKFT-derived nonlocal damping tensor in the 2D FI $\lambda_{\mathbf{R}}$, where $\mathbf{R} = (X, Y, Z)$ is the relative vector between two sites within the FI, covered by a NM [Eq. (5)], HM [Eqs. (8)], or AM [Eqs. (9)] metallic overlayer. (e) Wave-vector-dependent damping $\Gamma_{\mathbf{q}}$ of SWs due to the NM overlayer, where the gray line is based on Eq. (6) in the continuous limit [66] and the other two lines are numerical solutions of the extended LLG equation (1) for discrete lattices of LMMs within the FI. The dotted line in (e) is obtained in the absence of nonlocal damping ($\eta = 0$), which is flat at small q.

IV. RESULTS FOR A FI/HM BILAYER

Heavy metals (such as often-employed Pt, W, and Ta) exhibit strong SOC effects due to their large atomic number. We mimic their presence at the FI/HM interface [56] by using 2D energy-momentum dispersion $\epsilon_{\mathbf{k}} = t_0(k_x^2 + k_y^2) + t_{\text{SOC}}(\sigma^x k_y - \sigma^y k_x)$, which includes spin splitting due to the Rashba SOC [56,57]. Using this dispersion, Eq. (2) yields

$$\lambda_{\mathbf{R}}^{\text{HM}} = \begin{pmatrix} \lambda_{\mathbf{R}}^{xx} & \lambda_{\mathbf{R}}^{xy} & 0 \\ \lambda_{\mathbf{R}}^{xy} & \lambda_{\mathbf{R}}^{yy} & 0 \\ 0 & 0 & \lambda_{\mathbf{R}}^{zz} \end{pmatrix} \quad (7)$$

for the nonlocal damping tensor. Its components are, in general, different from each other:

$$\lambda_{\mathbf{R}}^{xx} = \frac{J_{sd}^2}{4\pi} \left[\left(\frac{k_{F\uparrow}}{v_{F\uparrow}} J_0(k_{F\uparrow}R) + \frac{k_{F\downarrow}}{v_{F\downarrow}} J_0(k_{F\downarrow}R) \right)^2 \right.$$
$$\left. + \cos(2\theta) \left(\frac{k_{F\uparrow}}{v_{F\uparrow}} J_1(k_{F\uparrow}R) - \frac{k_{F\downarrow}}{v_{F\downarrow}} J_1(k_{F\downarrow}R) \right)^2 \right], \quad (8a)$$

$$\lambda_{\mathbf{R}}^{yy} = \frac{J_{sd}^2}{4\pi} \left[\left(\frac{k_{F\uparrow}}{v_{F\uparrow}} J_0(k_{F\uparrow}R) + \frac{k_{F\downarrow}}{v_{F\downarrow}} J_0(k_{F\downarrow}R) \right)^2 \right.$$
$$\left. - \cos(2\theta) \left(\frac{k_{F\uparrow}}{v_{F\uparrow}} J_1(k_{F\uparrow}R) - \frac{k_{F\downarrow}}{v_{F\downarrow}} J_1(k_{F\downarrow}R) \right)^2 \right], \quad (8b)$$

$$\lambda_{\mathbf{R}}^{zz} = \frac{J_{sd}^2}{4\pi} \left[\left(\frac{k_{F\uparrow}}{v_{F\uparrow}} J_0(k_{F\uparrow}R) + \frac{k_{F\downarrow}}{v_{F\downarrow}} J_0(k_{F\downarrow}R) \right)^2 \right.$$
$$\left. - \left(\frac{k_{F\uparrow}}{v_{F\uparrow}} J_1(k_{F\uparrow}R) - \frac{k_{F\downarrow}}{v_{F\downarrow}} J_1(k_{F\downarrow}R) \right)^2 \right], \quad (8c)$$

$$\lambda_{\mathbf{R}}^{xy} = -\frac{J_{sd}^2 \sin(2\theta)}{4\pi} \left(\frac{k_{F\uparrow}}{v_{F\uparrow}} J_1(k_{F\uparrow}R) - \frac{k_{F\downarrow}}{v_{F\downarrow}} J_1(k_{F\downarrow}R) \right)^2, \quad (8d)$$

where $k_{F\uparrow}$ and $k_{F\downarrow}$ are the spin-split Fermi wave vectors [Fig. 1(b)] and θ is the relative orientation angle [Fig. 1(b)] between the SW wave vector $\mathbf{q}$ and the k_x direction. Thus, the nonlocal damping tensor in Eq. (7) generated by the HM overlayer is anisotropic in spin due to its different diagonal elements, as well as nonzero off-diagonal elements. It is also anisotropic in space due to its dependence on the angle θ. Its elements [Eqs. (8)] are plotted in Figs. 3(b), 3(c), 3(f), and 3(g) using $t_{\text{SOC}} = 0.3t_0$ and reduce to the FI/NM case if $t_{\text{SOC}} = 0$. They may become negative, signifying the possibility of antidamping torque [23] exerted by conduction electrons. However, the dominant effect of nearby LMMs and the presence of the local scalar α_G ensure that LMM dynamics is damped overall. Although there is no closed expression for the SW dispersion in the presence of anisotropic $\lambda_{\mathbf{R}}^{\text{HM}}$, we can still extract SW damping $\Gamma_{\mathbf{q}}$ induced by an HM overlayer from the exponential decay of the SW amplitude in numerical integration of the extended LLG equation (1) using SW initial conditions with varying $\mathbf{q}$. For an HM overlayer with realistic [56,57] $t_{\text{SOC}} = 0.1t_0$ the results in Fig. 4(a) are very similar to those obtained for the NM overlayer with the same Fermi energy. Also, the spatial anisotropy of $\lambda_{\mathbf{R}}^{\text{HM}}$ does not translate into θ dependence of the SW damping.

V. RESULTS FOR A FI/AM BILAYER

Altermagnets [58,59] are a novel class of antiferromagnets with spin-split electronic energy-momentum dispersion despite zero net magnetization or the lack of SOC. They are currently being intensely explored as a new resource for spintronics [63,69,70] and magnonics [71,72]. A simple model for an AM overlayer employs energy-momentum dispersion $\epsilon_{\mathbf{k}\sigma} = t_0(k_x^2 + k_y^2) - t_{\text{AM}}\sigma(k_x^2 - k_y^2)$ [58,59], where t_{AM} is the parameter characterizing anisotropy in the AM.
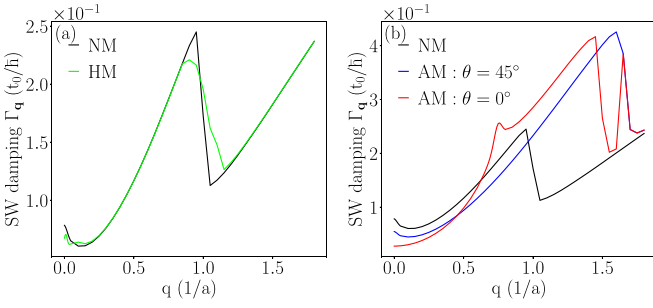
FIG. 4. (a) Wave-vector-dependent damping $\Gamma_{\mathbf{q}}$ of SWs under a NM or HM overlayer with Rashba SOC of strength $t_{SOC} = 0.1t_0$. (b) $\Gamma_{\mathbf{q}}$ of SWs under an AM overlayer with $t_{AM} = 0.8t_0$ for different relative orientations of the FI and AM layers measured by angle θ (Fig. 1). All calculations employ $\eta = 0.1$ and Fermi energy $\varepsilon_F = 0.25t_0$.

The corresponding $\lambda_{\mathbf{R}}^{AM} = \mathrm{diag}(\lambda_{\mathbf{R}}^{\perp}, \lambda_{\mathbf{R}}^{\perp}, \lambda_{\mathbf{R}}^{\parallel})$ tensor has three components, which we derive from Eq. (2) as

$$\lambda_{\mathbf{R}}^{\perp} = \frac{J_{sd}^2}{4\pi A_+ A_-}\left[J_0^2\left(\sqrt{\frac{\epsilon_F}{t_0}}R_+\right) + J_0^2\left(\sqrt{\frac{\epsilon_F}{t_0}}R_-\right)\right], \quad (9a)$$

$$\lambda_{\mathbf{R}}^{\parallel} = \frac{J_{sd}^2}{2\pi A_+ A_-}J_0\left(\sqrt{\frac{\epsilon_F}{t_0}}R_+\right)J_0\left(\sqrt{\frac{\epsilon_F}{t_0}}R_-\right), \quad (9b)$$

where $A_{\pm} = t_0 \pm t_{AM}$ and $R_{\pm}^2 = X^2/A_{\pm} + Y^2/A_{\mp}$ is the anisotropically rescaled norm of $\mathbf{R}$. They are plotted in Figs. 3(d) and 3(h), demonstrating that $\lambda_{\mathbf{R}}^{AM}$ is highly anisotropic in space and spin due to the importance of the angle θ [69,73,74]. The components of the nonlocal damping tensor can also take negative values, akin to the case of $\lambda_{\mathbf{R}}^{HM}$. It is interesting to note that along the direction of $\theta = 45°$ [gray dashed lines in Figs. 3(d) and 3(h)], $\lambda_{\mathbf{R}}^{\perp} = \lambda_{\mathbf{R}}^{\parallel}$, so the nonlocal damping tensor is isotropic in spin. The SW damping $\Gamma_{\mathbf{q}}$ induced by an AM overlayer is extracted from numerical integration of the extended LLG equation (1) and plotted in Fig. 4(b). Using a relatively large, but realistic [58], AM parameter $t_{AM} = 0.8t_0$, the SW damping along $\theta = 0°$ for experimentally relevant small wave vectors is reduced when compared to the one due to the NM overlayer by up to 65% [Fig. 4(b)]. Additional nontrivial features are observed at higher $|\mathbf{q}|$, such as being operative for a greater range of wave vectors with maxima around $|\mathbf{q}| = 2\sqrt{\epsilon_F/t_0}$ and $|\mathbf{q}| = 3\sqrt{\epsilon_F/t_0}$. Remarkably, these peaks vanish for wave vectors along the isotropic direction $\theta = 45°$ [Fig. 4(b)].

VI. CONCLUSIONS

In conclusion, using a SKFT-derived nonlocal damping tensor [45], we demonstrated a rigorous path to obtain wave vector damping of SWs in magnetic insulators due to interaction with the conduction electrons of the metallic overlayer, a setup often encountered in magnonics [15–19,39], where such SW damping was directly measured in very recent experiments [26–29]. Our analytical expressions [Eqs. (5), (7), and (9)] for the nonlocal damping tensor—using simple models of NM, HM, and AM overlayers as input—can be directly plugged into atomistic spin dynamics simulations [30]. For more complicated band structures of metallic overlayers, one

can compute $\lambda_{\mathbf{R}}$ numerically via Eq. (2), including a combination with first-principles calculations [37].

The interfacial J_{sd} coupling was estimated to be 50 meV in YIG/Pt [75] and as high as 400 meV in YIG/Au [76], accounting for the 100-fold increase [26–29] in SW damping underneath a metallic overlayer (see Appendix A for more details). This increase is incompatible with prior classical theories of nonlocal damping [43,44], emphasizing the necessity of the quantum mechanical foundations of our SKFT-based approach. Since we find that $\lambda_{\mathbf{R}}^{HM,AM}$ is highly anisotropic in spin and space, the corresponding SW damping $\Gamma_{\mathbf{q}}$ thus understood microscopically from SKFT allows us to propose how to manipulate it (Fig. 4). For example, by using a HM or AM overlayer and by changing their relative orientation with respect to the FI layer, $\Gamma_{\mathbf{q}}$ can be reduced by up to 65% for small wave vectors $\mathbf{q}$ (Fig. 4), which could be of great interest to magnonics experiments and applications.

APPENDIX A: ESTIMATING THE MAGNITUDE OF SW DAMPING FOR A REALISTIC YIG/Au BILAYER FROM SKFT VERSUS FROM REFERENCE [43]

The strength of the SKFT-derived nonlocal damping that gives rise to the wave-vector-dependent damping of SWs is given by the dimensionless parameter

$$\eta = \frac{k_F^2 J_{sd}^2 a_{Au}^4}{2\pi \hbar^2 v_F^2}, \quad (A1)$$

where J_{sd} is the interfacial sd exchange coupling; k_F and v_F are the norm of the Fermi wave vector and Fermi velocity, respectively; and a_{Au} is the distance between nearest neighbors (NNs) in Au. Reference [76], based on a many-body model, estimated the J_{sd} coupling for a YIG/Au bilayer to be

$$J_{sd} = 0.33 \times 2\pi t_0 a_{Au} \frac{\sqrt{g_{\uparrow\downarrow}}}{s}, \quad (A2)$$

where t_0 is the NN hopping parameter of Au, $g_{\uparrow\downarrow}$ is the spin-mixing conductance at the interface, and s is the spin quantum number of YIG. The latter is estimated to be $s = M_s a_{YIG} a_{Au}^2/\hbar\gamma_e$, where $M_s = 1.6 \times 10^5$ A/m is the saturation magnetization of YIG, $a_{YIG} = 12$ Å is the lattice constant of YIG, and $\gamma_e = 1.76 \times 10^{11}$ rad s^{-1} T^{-1} is the gyromagnetic ratio of the electron. The NN distance in Au is $a_{Au} = \sqrt{0.63/g_{sh}}$, where $g_{sh} = 12$ nm^{-2} is the Sharvin conductance of Au. Therefore, the spin quantum number of YIG is approximately $s = 0.54$, or about spin 1/2.

Next, the Au hopping parameter is estimated to be $t_0 = \varepsilon_F/12$, where $\varepsilon_F = 5.5$ eV is the Fermi energy of Au. This allows us to determine $t_0 = 0.46$ eV, as well as the norm of the Fermi wave vector $k_F = 10.69$ nm^{-1} and Fermi velocity 1.6×10^6 m/s. The spin-mixing conductance at the interface $g_{\uparrow\downarrow}$ is reported [76] to be between 1.2 and 6 nm^{-1}: we use the lower bound of $g_{\uparrow\downarrow} = 1.2$ nm^{-1}. Plugging that into Eq. (A2), we get a lower bound for $J_{sd} = 0.44$ eV. Then,
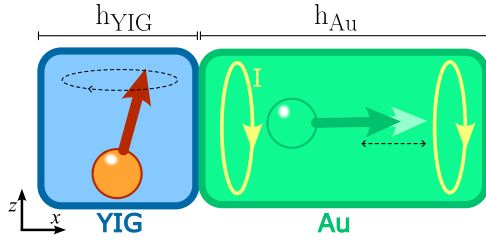
FIG. 5. Schematic diagram of a classical precessing localized magnetic moment in the YIG layer that induces eddy currents I within an Au overlayer, as used in the theory of Ref. [26].

in turn, plugging that into Eq. (A1) yields $\eta = 8.6 \times 10^{-3}$. Let us recall that the local scalar Gilbert damping of YIG is $\sim 10^{-4}$, meaning that the effective damping under an Au overlayer is predicted to be *at least* ~ 80 times stronger than in pure YIG. This is fully compatible with recent NV magnetometry measurements that observed a 100-fold increase. In contrast, some theories based on classical electrodynamics [43,44] predict a modest approximately twofold increase. Crucially, these references employ the same spin-mixing conductance of $g_{\uparrow\downarrow} = 1.2$ nm^{-1} as the key quantity to obtain the result.

APPENDIX B: ESTIMATING THE MAGNITUDE OF SW DAMPING FROM REF. [26] DUE TO BACKACTION OF EDDY CURRENTS IN Au GENERATED BY DYNAMICAL MAGNETIC MOMENTS OF YIG

The NV magnetometry experiments showing a dramatic increase in SW damping [26] employ a classical electrodynamics framework in which precessing magnetic moments in YIG induce eddy currents in the Au overlayer. The eddy currents, in turn, generate a magnetic moment whose magnetic field exerts a dampinglike torque on the localized magnetic moments of the YIG. However, Ref. [26] left the damping as a free parameter. Here, we compute the damping parameter of a single classical precessing moment based on realistic material parameters. The geometry we consider is depicted in Fig. 5: a cube of YIG of thickness $h_{\text{YIG}} = 235$ nm under a layer of Au of thickness $h_{\text{Au}} = 200$ nm. The magnetization of the YIG cube is averaged to determine a single magnetic dipole moment $m_{\text{YIG}} = M_s h_{\text{YIG}}^3$ that exhibits precessing motion according to $\mathbf{m}_{\text{YIG}} = m_{\text{YIG}}(\sin\theta \sin\omega t, \sin\theta \cos\omega t, \cos\theta)$. The precession frequency is $\omega/2\pi = 2$ GHz, and θ is the angle of the magnetic moment with the z axis.

The magnetic field generated by a localized magnetic dipole [77] is given by

$$\mathbf{B}(\mathbf{r}) = \frac{\mu_0}{4\pi}\left[\frac{\mathbf{e}_r(\mathbf{e}_r \cdot \partial_t^2\mathbf{m}) - \partial_t^2\mathbf{m}}{rc^2} + \frac{3\mathbf{e}_r(\mathbf{e}_r \cdot \mathbf{M}) - \mathbf{M}}{r^3}\right],$$
(B1)

where c is the speed of light, $\mathbf{e}_r$ is the radial unit vector at position $\mathbf{r}$, $\mathbf{M} = \mathbf{m} + r\partial_t\mathbf{m}/c$, and retardation effects can be ignored since $\omega h_{\text{Au}}/c \sim 10^{-6}$. Assuming the Au layer is thin enough, only the x component of the magnetic field radiated by $\mathbf{m}_{\text{YIG}}$, B_{YIG}^x, contributes to the flux through the Au. This component is obtained from Eq. (B1) as

$$B_{\text{YIG}}^x(x, y = 0, z = 0) = \frac{\mu_0 m_{\text{YIG}}}{2\pi x^3}\sin\theta \cos\omega t,$$
(B2)

where terms of order $\omega x/c$ are neglected. Thus, the electromotive force ϵ induced in the Au is given by

$$\epsilon = h_{\text{YIG}}^2 \int_{\text{Au}} dx\, \partial_t B_{\text{YIG}}^x(x, y = 0, z = 0),$$
(B3)

where the flux is integrated over the thickness of the Au layer. Thus, the circulating eddy currents are $I = \epsilon/\rho_{\text{Au}} = I_0\sin\omega t$, where $\rho_{\text{Au}} = 11$ nΩ m is the resistivity of the Au thin film at room temperature [78]. Such currents generate an induced magnetic dipole $\mathbf{m}_{\text{Au}} = I_0 h_{\text{YIG}}^2\sin\omega t\mathbf{e}_x$, whose generated magnetic field at the location of the YIG magnetic moment is obtained from Eq. (B1) as

$$\mathbf{B}_{\text{Au}} = \frac{4\mu_0 I_0 h_{\text{YIG}}^2\sin\omega t}{\pi(h_{\text{Au}} + h_{\text{YIG}})^3}\mathbf{e}_x.$$
(B4)

The torque exerted by this field can be included in the LLG equations for a precessing magnetic moment as an additional term, yielding

$$\partial_t\mathbf{m}_{\text{YIG}} = -\gamma_e\mathbf{m}_{\text{YIG}} \times \mathbf{B}_{\text{ext}} + \alpha_G\mathbf{m}_{\text{YIG}} \times \partial_t\mathbf{m}_{\text{YIG}}$$
$$+ \alpha_1\mathbf{m}_{\text{YIG}} \times (\partial_t\mathbf{m}_{\text{YIG}} \cdot \mathbf{e}_x)\mathbf{e}_x,$$
(B5)

where α_G is the conventional Gilbert damping scalar and $\alpha_1 = \gamma_e B_{\text{Au}}/\omega$ is the additional damping due to the eddy currents. This parameter is, approximately, $\alpha_1 \approx 0.012$, compatible with the experimental observations [26] and 100 times larger than intrinsic $\alpha_G = 10^{-4}$. However, Eq. (B5) is the usual LLG equation with traditional uniform Gilbert damping, whose value is anisotropically enhanced [second term on the right-hand side of Eq. (B5)] by the eddy-current backaction. It has been understood [10,36] that simple renormalization of the Gilbert damping constant, which is the same for all SW modes at different wave vectors, is insufficient to produce wave-vector-dependent damping. Instead, wave-vector-dependent SW damping requires a nonlocal damping term in the LLG equation, which is coordinate and magnetization texture dependent. Deriving such a nonlocal damping term cannot be achieved using simple physical arguments leading to Eq. (B5); instead, one needs more microscopic approaches [10,11,34–36], one of which (perhaps the most rigorous due to being benchmarked by numerically exact calculations [45,64]) is provided by our SKFT-based formulation [45].

[1] Y. Li and W. E. Bailey, Wave-number-dependent Gilbert damping in metallic ferromagnets, Phys. Rev. Lett. **116**, 117602 (2016).

[2] L. Chen, C. Mao, J.-H. Chung, M. B. Stone, A. I. Kolesnikov, X. Wang, N. Murai, B. Gao, O. Delaire, and P. Dai, Anisotropic magnon damping by zero-temperature quantum

fluctuations in ferromagnetic CrGeTe₃, Nat. Commun. **13**, 4037 (2022).

[3] P. Dai, H. Y. Hwang, J. Zhang, J. A. Fernandez-Baca, S.-W. Cheong, C. Kloc, Y. Tomioka, and Y. Tokura, Magnon damping by magnon-phonon coupling in manganese perovskites, Phys. Rev. B **61**, 9553 (2000).

[4] S. P. Bayrakci, D. A. Tennant, P. Leininger, T. Keller, M. C. R. Gibson, S. D. Wilson, R. J. Birgeneau, and B. Keimer, Lifetimes of antiferromagnetic magnons in two and three dimensions: Experiment, theory, and numerics, Phys. Rev. Lett. **111**, 017204 (2013).

[5] M. E. Zhitomirsky and A. L. Chernyshev, *Colloquium*: Spontaneous magnon decays, Rev. Mod. Phys. **85**, 219 (2013).

[6] U. Bajpai, A. Suresh, and B. K. Nikolić, Quantum many-body states and Green's functions of nonequilibrium electron-magnon systems: Localized spin operators versus their mapping to Holstein-Primakoff bosons, Phys. Rev. B **104**, 184425 (2021).

[7] R. L. Smit, S. Keupert, O. Tsyplyatyev, P. A. Maksimov, A. L. Chernyshev, and P. Kopietz, Magnon damping in the zigzag phase of the Kitaev-Heisenberg-Γ model on a honeycomb lattice, Phys. Rev. B **101**, 054424 (2020).

[8] S. M. Winter, K. Riedl, P. A. Maksimov, A. L. Chernyshev, A. Honecker, and R. Valenti, Breakdown of magnons in a strongly spin-orbital coupled magnet, Nat. Commun. **8**, 1152 (2017).

[9] M. Gohlke, A. Corticelli, R. Moessner, P. A. McClarty, and A. Mook, Spurious symmetry enhancement in linear spin wave theory and interaction-induced topology in magnons, Phys. Rev. Lett. **131**, 186702 (2023).

[10] E. M. Hankiewicz, G. Vignale, and Y. Tserkovnyak, Inhomogeneous Gilbert damping from impurities and electron-electron interactions, Phys. Rev. B **78**, 020404(R) (2008).

[11] Y. Tserkovnyak, E. M. Hankiewicz, and G. Vignale, Transverse spin diffusion in ferromagnets, Phys. Rev. B **79**, 094415 (2009).

[12] P. Nikolić, Universal spin wave damping in magnetic Weyl semimetals, Phys. Rev. B **104**, 024414 (2021).

[13] M. Isoda, Spin-wave damping in itinerant electron ferromagnets, J. Phys.: Condens. Matter **2**, 3579 (1990).

[14] P. Buczek, A. Ernst, P. Bruno, and L. M. Sandratskii, Energies and lifetimes of magnons in complex ferromagnets: A first-principle study of Heusler alloys, Phys. Rev. Lett. **102**, 247206 (2009).

[15] A. Chumak, V. Vasyuchka, A. Serga, and B. Hillebrands, Magnon spintronics, Nat. Phys. **11**, 453 (2015).

[16] G. Csaba, A. Papp, and W. Porod, Perspectives of using spin waves for computing and signal processing, Phys. Lett. A **381**, 1471 (2017).

[17] A. V. Chumak, Fundamentals of magnon-based computing, arXiv:1901.08934.

[18] A. V. Chumak, P. Kabos, M. Wu, C. Abert, C. Adelmann, A. O. Adeyeye, J. Akerman, F. G. Aliev, A. Anane, A. Awad *et al.*, Advances in magnetics roadmap on spin-wave computing, IEEE Trans. Magn. **58**, 1 (2022).

[19] A. Mahmoud, F. Ciubotaru, F. Vanderveken, A. V. Chumak, S. Hamdioui, C. Adelmann, and S. Cotofana, Introduction to spin wave computing, J. Appl. Phys. **128**, 161101 (2020).

[20] A. Hamadeh, O. d'Allivy Kelly, C. Hahn, H. Meley, R. Bernard, A. H. Molpeceres, V. V. Naletov, M. Viret, A. Anane, V. Cros *et al.*, Full control of the spin-wave damping in a magnetic insulator using spin-orbit torque, Phys. Rev. Lett. **113**, 197203 (2014).

[21] A. Akhiezer, V. Baryakhtar, and S. Peletminskii, Coherent amplification of spin waves, Sov. Phys. JETP **18**, 235 (1964).

[22] M. Evelt, V. E. Demidov, V. Bessonov, S. O. Demokritov, J. L. Prieto, M. Muñoz, J. B. Youssef, V. V. Naletov, G. de Loubens, O. Klein *et al.*, High-efficiency control of spin-wave propagation in ultra-thin yttrium iron garnet by the spin-orbit torque, Appl. Phys. Lett. **108**, 172406 (2016).

[23] V. E. Demidov, S. Urazhdin, A. Anane, V. Cros, and S. O. Demokritov, Spin–orbit-torque magnonics, J. Appl. Phys. **127**, 170901 (2020).

[24] D. Breitbach, M. Schneider, B. Heinz, F. Kohl, J. Maskill, L. Scheuer, R. O. Serha, T. Brächer, B. Lägel, C. Dubs *et al.*, Stimulated amplification of propagating spin waves, Phys. Rev. Lett. **131**, 156701 (2023).

[25] F. Bloch, Zur theorie des ferromagnetismus, Z. Phys. **61**, 206 (1930).

[26] I. Bertelli, B. G. Simon, T. Yu, J. Aarts, G. E. W. Bauer, Y. M. Blanter, and T. van der Sar, Imaging spin-wave damping underneath metals using electron spins in diamond, Adv. Quantum Technol. **4**, 2100094 (2021).

[27] S. Mae, R. Ohshima, E. Shigematsu, Y. Ando, T. Shinjo, and M. Shiraishi, Influence of adjacent metal films on magnon propagation in Y₃Fe₅O₁₂, Phys. Rev. B **105**, 104415 (2022).

[28] A. Krysztofik, N. Kuznetsov, H. Qin, L. Flajšman, E. Coy, and S. van Dijken, Tuning of magnetic damping in Y₃Fe₅O₁₂/metal bilayers for spin-wave conduit termination, Materials **15**, 2814 (2022).

[29] R. O. Serha, D. A. Bozhko, M. Agrawal, R. V. Verba, M. Kostylev, V. I. Vasyuchka, B. Hillebrands, and A. A. Serga, Low-damping spin-wave transmission in YIG/Pt-interfaced structures, Adv. Mater. Interfaces **9**, 2201323 (2022).

[30] R. Evans, W. Fan, P. Chureemart, T. Ostler, M. O. Ellis, and R. Chantrell, Atomistic spin model simulations of magnetic nanomaterials, J. Phys.: Condens. Matter **26**, 103202 (2014).

[31] S.-K. Kim, Micromagnetic computer simulations of spin waves in nanometre-scale patterned magnetic elements, J. Phys. D **43**, 264004 (2010).

[32] T. Gilbert, A phenomenological theory of damping in ferromagnetic materials, IEEE Trans. Magn. **40**, 3443 (2004).

[33] W. M. Saslow, Landau-Lifshitz or Gilbert damping? That is the question, J. Appl. Phys. **105**, 07D315 (2009).

[34] S. Zhang and S. S.-L. Zhang, Generalization of the Landau-Lifshitz-Gilbert equation for conducting ferromagnets, Phys. Rev. Lett. **102**, 086601 (2009).

[35] H. Y. Yuan, Z. Yuan, K. Xia, and X. R. Wang, Influence of nonlocal damping on the field-driven domain wall motion, Phys. Rev. B **94**, 064415 (2016).

[36] R. Verba, V. Tiberkevich, and A. Slavin, Damping of linear spin-wave modes in magnetic nanostructures: Local, nonlocal, and coordinate-dependent damping, Phys. Rev. B **98**, 104408 (2018).

[37] Z. Lu, I. P. Miranda, S. Streib, M. Pereiro, E. Sjöqvist, O. Eriksson, A. Bergman, D. Thonig, and A. Delin, Influence of nonlocal damping on magnon properties of ferromagnets, Phys. Rev. B **108**, 014433 (2023).

[38] K. Gilmore, Y. U. Idzerda, and M. D. Stiles, Identification of the dominant precession-damping mechanism in Fe, Co, and

Ni by first-principles calculations, Phys. Rev. Lett. **99**, 027204 (2007).

[39] A. A. Serga, A. V. Chumak, and B. Hillebrands, YIG magnonics, J. Phys. D **43**, 264002 (2010).

[40] P. Trempler, R. Dreyer, P. Geyer, C. Hauser, G. Woltersdorf, and G. Schmidt, Integration and characterization of micron-sized YIG structures with very low Gilbert damping on arbitrary substrates, Appl. Phys. Lett. **117**, 232401 (2020).

[41] F. Casola, T. van der Sar, and A. Yacoby, Probing condensed matter physics with magnetometry based on nitrogen-vacancy centres in diamond, Nat. Rev. Mater. **3**, 17088 (2018).

[42] I. N. Krivorotov, D. V. Berkov, N. L. Gorn, N. C. Emley, J. C. Sankey, D. C. Ralph, and R. A. Buhrman, Large-amplitude coherent spin waves excited by spin-polarized current in nanoscale spin valves, Phys. Rev. B **76**, 024418 (2007).

[43] A. Kapelrud and A. Brataas, Spin pumping and enhanced Gilbert damping in thin magnetic insulator films, Phys. Rev. Lett. **111**, 097602 (2013).

[44] H. Skarsvåg, A. Kapelrud, and A. Brataas, Spin waves in ferromagnetic insulators coupled via a normal metal, Phys. Rev. B **90**, 094418 (2014).

[45] F. Reyes-Osorio and B. K. Nikolić, Gilbert damping in metallic ferromagnets from Schwinger-Keldysh field theory: Intrinsically nonlocal, nonuniform, and made anisotropic by spin-orbit coupling, Phys. Rev. B **109**, 024413 (2024).

[46] A. Kamenev, *Field Theory of Non-Equilibrium Systems* (Cambridge University Press, Cambridge, 2023).

[47] M. D. Petrović, B. S. Popescu, U. Bajpai, P. Plecháč, and B. K. Nikolić, Spin and charge pumping by current-driven magnetic domain wall motion: A self-consistent multiscale time-dependent-quantum/time-dependent-classical approach, Phys. Rev. Appl. **10**, 054038 (2018).

[48] U. Bajpai and B. K. Nikolić, Time-retarded damping and magnetic inertia in the Landau-Lifshitz-Gilbert equation self-consistently coupled to electronic time-dependent nonequilibrium Green functions, Phys. Rev. B **99**, 134409 (2019).

[49] M. D. Petrović, U. Bajpai, P. Plecháč, and B. K. Nikolić, Annihilation of topological solitons in magnetism with spin-wave burst finale: Role of nonequilibrium electrons causing nonlocal damping and spin pumping over ultrabroadband frequency range, Phys. Rev. B **104**, L020407 (2021).

[50] A. Suresh, U. Bajpai, and B. K. Nikolić, Magnon-driven chiral charge and spin pumping and electron-magnon scattering from time-dependent quantum transport combined with classical atomistic spin dynamics, Phys. Rev. B **101**, 214412 (2020).

[51] F. M. Haehl, R. Loganayagam, and M. Rangamani, Schwinger-Keldysh formalism. Part I: BRST symmetries and superspace, J. High Energ. Phys. 06 (2017) 069.

[52] F. M. Haehl, R. Loganayagam, and M. Rangamani, Schwinger-Keldysh formalism. Part II: Thermal equivariant cohomology, J. High Energ. Phys. 06 (2017) 070.

[53] J. Berges, Nonequilibrium quantum fields: From cold atoms to cosmology, arXiv:1503.02907.

[54] J. Anders, C. R. J. Sait, and S. A. R. Horsley, Quantum Brownian motion for magnets, New J. Phys. **24**, 033020 (2022).

[55] S. Leiva M., S. A. Díaz, and A. S. Nunez, Origin of the magnetoelectric couplings in the spin dynamics of molecular magnets, Phys. Rev. B **107**, 094401 (2023).

[56] G. Bihlmayer, P. Noël, D. V. Vyalikh, E. V. Chulkov, and A. Manchon, Rashba-like physics in condensed matter, Nat. Rev. Phys. **4**, 642 (2022).

[57] A. Manchon, H. C. Koo, J. Nitta, S. M. Frolov, and R. A. Duine, New perspectives for Rashba spin–orbit coupling, Nat. Mater. **14**, 871 (2015).

[58] L. Šmejkal, J. Sinova, and T. Jungwirth, Emerging research landscape of altermagnetism, Phys. Rev. X **12**, 040501 (2022).

[59] L. Šmejkal, A. B. Hellenes, R. González-Hernández, J. Sinova, and T. Jungwirth, Giant and tunneling magnetoresistance in unconventional collinear antiferromagnets with nonrelativistic spin-momentum coupling, Phys. Rev. X **12**, 011028 (2022).

[60] M. Hiraishi, H. Okabe, A. Koda, R. Kadono, T. Muroi, D. Hirai, and Z. Hiroi, Nonmagnetic Ground State in RuO_2 Revealed by Muon Spin Rotation, Phys. Rev. Lett. **132**, 166702 (2024).

[61] A. Smolyanyuk, I. I. Mazin, L. Garcia-Gassull, and R. Valentí, Fragility of the magnetic order in the prototypical altermagnet RuO_2, Phys. Rev. B **109**, 134424 (2024).

[62] S. G. Jeong, I. H. Choi, S. Nair, L. Buiarelli, B. Pourbahari, J. Young Oh, N. Bassim, A. Seo, W. S. Choi, R. M. Fernandes, T. Birol, L. Zhao, J. S. Lee, and B. Jalan, Altermagnetic Polar Metallic phase in Ultra-Thin Epitaxially-Strained RuO_2 Films, arXiv:2405.05838.

[63] H. Bai, Y. C. Zhang, Y. J. Zhou, P. Chen, C. H. Wan, L. Han, W. X. Zhu, S. X. Liang, Y. C. Su, X. F. Han *et al.*, Efficient spin-to-charge conversion via altermagnetic spin splitting effect in antiferromagnet RuO_2, Phys. Rev. Lett. **130**, 216701 (2023).

[64] M. Sayad and M. Potthoff, Spin dynamics and relaxation in the classical-spin Kondo-impurity model beyond the Landau-Lifshitz-Gilbert equation, New J. Phys. **17**, 113058 (2015).

[65] D. Ralph and M. Stiles, Spin transfer torques, J. Magn. Magn. Mater. **320**, 1190 (2008).

[66] B. Halperin and P. Hohenberg, Hydrodynamic theory of spin waves, Phys. Rev. **188**, 898 (1969).

[67] B. Gaury, J. Weston, M. Santin, M. Houzet, C. Groth, and X. Waintal, Numerical simulations of time-resolved quantum electronics, Phys. Rep. **534**, 1 (2014).

[68] M. Madami, S. Bonetti, G. Consolo, S. Tacchi, G. Carlotti, G. Gubbiotti, F. B. Mancoff, M. A. Yar, and J. Åkerman, Direct observation of a propagating spin wave induced by spin-transfer torque, Nat. Nanotechnol. **6**, 635 (2011).

[69] C. Sun and J. Linder, Spin pumping from a ferromagnetic insulator into an altermagnet, Phys. Rev. B **108**, L140408 (2023).

[70] R.-W. Zhang, C. Cui, R. Li, J. Duan, L. Li, Z.-M. Yu, and Y. Yao, Predictable gate-field control of spin in altermagnets with spin-layer coupling, Phys. Rev. Lett. **133**, 056401 (2024).

[71] L. Šmejkal, A. Marmodoro, K.-H. Ahn, R. González-Hernández, I. Turek, S. Mankovsky, H. Ebert, S. W. D'Souza, O. Šipr, J. Sinova, and T. Jungwirth, Chiral magnons in altermagnetic RuO_2, Phys. Rev. Lett. **131**, 256703 (2023).

[72] Z. Jin, H. Yang, Z. Zeng, Y. Cao, and P. Yan, Cavity-induced strong magnon-magnon coupling in altermagnets, arXiv:2307.00909.

[73] M. Papaj, Andreev reflection at the altermagnet-superconductor interface, Phys. Rev. B **108**, L060508 (2023).

[74] C. Sun, A. Brataas, and J. Linder, Andreev reflection in altermagnets, Phys. Rev. B **108**, 054511 (2023).

[75] R. E. Troncoso, A. Brataas, and R. A. Duine, Many-body theory of spin-current driven instabilities in magnetic insulators, Phys. Rev. B **99**, 104426 (2019).

[76] N. Rohling, E. L. Fjærbu, and A. Brataas, Superconductivity induced by interfacial coupling to magnons, Phys. Rev. B **97**, 115401 (2018).

[77] D. J. Griffiths, Dynamic dipoles, Am. J. Phys. **79**, 867 (2011).

[78] J. R. Sambles, K. C. Elsom, and D. J. Jarvis, The electrical resistivity of gold films, Philos. Trans. R. Soc. London, Ser. A **304**, 365 (1982).